Environmental Pollution 307 (2022) 119564

Contents lists available at ScienceDirect

Environmental Pollution

journal homepage: www.elsevier.com/locate/envpol

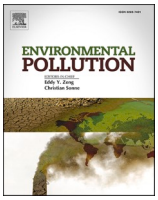

The respiratory cytotoxicity of typical organophosphorus flame retardants on five different respiratory tract cells: Which are the most sensitive one?☆

Jingyi Chen [a], Guiying Li [a,b], Hang Yu [a,b], Hongli Liu [a,b], Taicheng An [a,b,*]

[a] Guangdong-Hong Kong-Macao Joint Laboratory for Contaminants Exposure and Health, Guangdong Key Laboratory of Environmental Catalysis and Health Risk Control, Institute of Environmental Health and Pollution Control, Guangdong University of Technology, Guangzhou, 510006, China
[b] Guangzhou Key Laboratory of Environmental Catalysis and Pollution Control, Key Laboratory of City Cluster Environmental Safety and Green Development (Department of Education, China), School of Environmental Science and Engineering, Guangdong University of Technology, Guangzhou, 510006, China

ARTICLE INFO

Keywords:
Triphenyl phosphate
Respiratory tract cells
Oxidative stress
Cytotoxicity
Endoplasmic reticulum stress
Nrf2 signal pathway

ABSTRACT

Triphenyl phosphate (TPHP) is a frequently used flame retardant and indoor semi-volatile pollutant exposing humans with endocrinal disrupting effects. However, its respiratory tract toxicity remains unclear. Herein, we mainly focused on exploring the cytotoxicity of TPHP to the cells from five different parts of the human respiratory tract (from top to bottom): human nasal epithelial (HNEpC) cells, human bronchial epithelial (16HBE) cells, normal nasopharyngeal epithelial (NP69) cells, human lung epithelial cells (Beas-2B) cells, and human lung fibrocells (HFL1 cells) cells. The cell viability, micronucleus induction, endoplasmic reticulum stress gene, intracellular Ca^{2+} concentration, mitochondrial membrane potential (MMP) were investigated in short-term as well as extended exposure of TPHP. HFL1 and HNEpC cells were found to be irreversible damage, while other three type cells achieved homeostasis through self-rescue. Moreover, expression of downstream genes of Nrf2 signaling pathway were upregulated for 1.3–7.0 times and glutathione detoxification enzyme activity changed for 2–10 (U/mg protein) in HNEpC cells. Furthermore, the vascular endothelial growth factor (VEGF), a disease-related factor, increased 1.0–3.5-fold in HNEpC cells. RNA-sequencing results suggested that protein linkage recombination, molecular function regulation and metabolic processes signal pathway were all affected by TPHP exposure in HNEpC. This is a first report to compare respiratory cytotoxicity in whole human respiratory tract under OPFR exposure and found HNEpC cells were the most sensitive target of TPHP. Molecular biological mechanisms uncovered that TPHP exposure in HNEpC can induce the activation of MAPK signal pathway and demonstrate potential respiratory growth differentiation and stress disorder in human nasal cells upon TPHP exposure.

1. Introduction

The registration of polybrominated diphenylether production and usage leads to the adoption of organophosphorus flame retardants (OPFRs). The global production of OPFRs is range from 400,000 to 560,000 tons by 2021 (Dodson et al., 2012; Percy et al., 2020). OPFRs have recently been ubiquitous use in the production of plastics, textiles, building materials plasticizers, stabilizer, paints, lacquers and wetting agents (Li et al., 2020; Marklund et al., 2003; Wang et al., 2017). OPFRs are only mixed with polymer substrates rather than reacted with chemical bones, which give raise to the unstable structures and emission in many fashions freely into environment. Generally, higher concentrations of OPFRs were reported in indoor environments especially in the room with poor ventilation, because the products with OPFRs are frequently presented in indoor. Previous works investigated the pollution levels of different persistent organic compounds in various indoors including house, apartment, elementary school, office, and automotive environment, and found that the highest levels of OPFRs with the highest levels of triphenyl phosphate (TPHP) of 10700 ng/g were detected in residential apartments (Basaran and Civan, 2021; Strandberg et al., 2006). Therefore, OPFRs in the indoor environment mainly distributed in air, dust and surfaces will consequently exposed to the residents through various pathways such as inhalation (Al-Salem et al., 2019; Percy et al., 2020), ingestion and skin contact (Cao et al.,

☆ This paper has been recommended for acceptance by Wen Chen.

* Corresponding author. Guangdong-Hong Kong-Macao Joint Laboratory for Contaminants Exposure and Health, Guangdong Key Laboratory of Environmental Catalysis and Health Risk Control, Institute of Environmental Health and Pollution Control, Guangdong University of Technology, Guangzhou, 510006, China.
E-mail address: antc99@gdut.edu.cn (T. An).

https://doi.org/10.1016/j.envpol.2022.119564
Received 13 February 2022; Received in revised form 10 May 2022; Accepted 29 May 2022
Available online 30 May 2022

2019). More important, considerable number of studies suggested that relatively high level of OPFRs were detected in human body samples, including human serum (16.6 ng/mL), hand wipe (11.94 μg/sample) (Liu et al., 2017; Zhang et al., 2021), human urine (Tang et al., 2021) and worker's nails (2.68 μg/sample) in nail salon (Estill et al., 2021; Hanas et al., 2020) as well as some highly exposure area for example an e-waste dismantling park (Yue et al., 2022). A recent great review on *in vitro* and *in vivo* studies suggested that OPFRs have physiological toxicity, genetic poisonousness, metabolic disorders, endocrine dyscrasia to various organs of the human body (Al-Salem et al., 2019). For instance, TPHP significantly increases permeability of fish brain blood-brain barrier, activated neuroinflammatory response, therefore reduced learning and memory ability (Hong et al., 2018). The transcriptional changes were found in the HepG2 cells after tricresyl phosphate exposure (Al-Salem et al., 2019). OPFRs can adjust the blood-brain barrier permeability of mice through the transformation of glutamate, organic acids in the brain of mice, causing abnormalities in the hippocampus, cortex and thalamus of the brain (Liu et al., 2020; Yu et al., 2019).

Many studies indicated indoor dust ingestion as a main exposing pathway of human to OPFRs (Araki et al., 2014; Björnsdotter et al., 2018; Cao et al., 2019). A research on the outcomes of exposure to 11 OPFRs in indoor floor and multi-surface dust from 182 single-family residences was investigated in Japan, and found that OPFR levels were positively correlated with asthma and rhinitis (Araki et al., 2014). However, toxicological evidence of OPFRs on human respiratory tract cells has not been attempted yet. In addition, the enrichment ability of different organs to an organic pollutant is also discrepancy (Kempermann, 2019), due to the toxicity of an organic pollutant is also diverse in different organs (Hong et al., 2018; Qiu et al., 2021; Xiang et al., 2017) and even at different expoure concentration (Lu et al., 2021). When an organic pollutant is inhaled, it will pass through the whole respiratory tract from the upper to the lower respiratory tract. However, the target cells and cytotoxicity of pollutant might be different, which subsequently might lead to development of certain disease (Ning et al., 2020). Nevertheless, to date, such work in this field has not yet been attempted.

In this study, TPHP as a typical OPFRs was employed to screen cell viability, genotoxicity, endoplasmic reticulum stress, Ca^{2+} outflow, mitochondrial damage, Nrf2 pathway, and glutathione detoxification system of five different respiratory tract cells from the upper to the lower respiratory tract (human nasal epithelial (HNEpC) cells, human bronchial epithelial (16HBE) cells, normal nasopharyngeal epithelial (NP69) cells, human lung epithelial cells (Beas-2B) cells, and human lung fibrocells (HFL1) cells). The main purpose of this research is to explore differences in stress pattern in different respiratory tract cells and to find the potential target of the TPHP from the angle of whole respiratory tract. These initial findings will guide more in-depth insight into RNA-sequencing analysis and enrichment pathway analysis of TPHP in respiratory cells.

2. Materials and methods

2.1. Cell cultures and TPHP exposure

16HBE cells, Beas-2B cells, HFL1 cells, and HNEpC cells were from the Chinese Academy of Cell Resource Center (Shanghai, China). NP69 cell line was from ShenZhen coolrun life science technology. Beas-2B and 16HBE cells were cultured in DMEM medium (Gibco) supplemented with 10% fetal bovine serum (FBS) and 1% penicillin-streptomycin at 37 °C in a 5% CO_2 humidified cell culture incubator. HFL1, HNEpC and NP69 cells were cultured in F-12k medium, minimum Eagle's medium (MEM), RPMI 1640 medium, respectively, supplemented with 10% fetal bovine serum (FBS) and 1% penicillin-streptomycin. Details on cultivation methods are provided in supporting information (SI). Exposure concentrations of TPHP were selected as 0, 1, 10, 20, 50, 100, 200, 500, and 1000 μM for 24 and 72 h.

2.2. Detection of cell viability, lactate dehydrogenase (LDH), intracellular total reactive oxygen species (ROSs) and free cytosolic Ca^{2+}

Cell viability was analyzed using Cell Counting kit (CCK-8) cell viability assay kit (Beyotime Institute of Biotechnology, China). LDH leakage was determined using commercially available cell membrane lactate dehydrogenase toxicity kit (Jiancheng Bioengineering, Nanjing, China). ROSs were measured using 2′-7-'dichlorodihydro-fluoresceindiacetate (DCFH-DA) fluorescent probe (Beyotime Institute of Biotechnology, China). Fluo-4 AM fluorescent probe (Beyotime Institute of Biotechnology, China) was adopted to test free cytosolic Ca^{2+}. Detail information is provided in the SI.

After different concentrations of TPHP exposure in 96 pore plate, cells were rinsed twice with phosphate-buffered saline (PBS). Next, cells were incubated in DCFH-DA (2 mM) for 15 min at 37 °C dark incubator and washed twice with PBS, then detected using multimode reader (Varioskan flash, Thermo Fisher Scientific, USA) with excitation wavelength at 488 nm and emission wavelength at 525 nm (Al-Salem et al., 2019).

Intracellular Ca^{2+} was determined with a Fluo-4 AM fluorescent probe, and detected with fluorescence microscope (Beckman Coulter Gallios, USA) (Ji et al., 2008).

2.3. Determination of antioxidant liability level and cytokine test

After exposure, supernatant was sucked out into 1.5 mL centrifuge tubes and diluted 5 times with ultrapure water. The diluted supernatant was then used to measure activities of superoxide dismutase activity (SOD), catalase (CAT), glutathione peroxidase (GSH-Px), and glutathione reductase (GR) with Catalase Assay Kit (Beyotime Institute of Biotechnology, China), Superoxide Dismutase Assay Kit (Beyotime Institute of Biotechnology, China), Glutathione Peroxidase Assay Kit (Beyotime Institute of Biotechnology, China), Glutathione Reductase Assay Kit (Beyotime Institute of Biotechnology, China), respectively. Protein content of five different types of cells was analyzed using a BCA protein assay kit (Pierce, Thermo Scientific, USA) with bovine serum albumin as the standard.

Cytokine test of different cells was carried out according to instructions. Human vascular endothelial growth factor (VEGF), human matrix metalloproteinase (MMP-9), human tumor necrosis factor alpha (TNF-α), human granulocyt-macrophage colony-stimulating factor (GM-CSF), human transforming growth factor β1(TGF-β1), were adopted in HNEpC, 16HBE, NP-69, Beas-2B, and HFL1, respectively.

2.4. Micronucleus tests

The above five type cells were inoculated into 6-well plates with concentration of 10^5 cells per well. After 24 h culture, solvent control (DMSO) and 1, 10, 100 μM TPHP (DMSO concentration controlled within 0.1%) were added and exposed for 72 h. Three parallel experiments were set in each group. Washed twice with pre-cooled PBS, 500 μL trypsin was added into each well, digested in an incubator at 37 °C for 3 min, and 1 mL medium was supplemented into each well to terminate digestion. The mixed cells were blown and dispersed into single cells, and centrifuged for 5 min at 1000 rpm. Discard the medium, add 1 mL 0.075 mol/L KCl low permeability solution to 37 °C water baths for low permeability for 2.5 min, and quickly add 1 mL fixative solution into terminate the low permeability. Then centrifuge at 1000 rpm for 5 min, discard low osmotic solution and fixative solution, and dry in a cool and ventilated place for 10 min. Add an appropriate amount of fixative solution, and resuscitate the cells. Drop 40 μL cell suspension into the fixative solution and soak on the pre-cooled slides at −20 °C, then dry. The 1 × Giemsa working solution was placed in oven at 37 °C to heat up. Then, slides were added and dyed for 9 min. Total of 2000 intact interphase cells randomly entered field of vision and frequency of micronucleus cells was recorded in oil microscope. The criteria for

determining micronucleus were: round, oval or crescent shape, smooth edge, 1/16–1/3 of the diameter of main nucleus, completely separated from the main nucleus. The chromotropism was the same as or slightly lighter than main nucleus. In addition, aminobenzotriazole (ABT) or N-Acetyl-L-cysteine (NAC) were added into the above experiment to compare.

2.5. Mitochondrial membrane potential (MMP) examination

MMP was analyzed with fluorescent probe JC-1 (Beyotime Institute of Biotechnology, China), which was frequently used as an indicator of early apoptosis and depolarization of MMP (Zhao et al., 2018). Briefly, manner of cell culture and exposure regime was same with above. Cells were washed twice with ice-PBS, and then loaded with a fresh JC-1 fluorescent probe containing medium for 20 min at 37 °C. Finally, the fluorescence intensity of JC-1 was determined with an inverted fluorescence microscopy (Wang et al., 2018).

2.6. RNA separation and RNA-sequence

The five different cells were processed in the way described above. Total RNA was extracted from cells using Trizol reagent. RNA integrity was confirmed by A260/280 ratio, and the ratios of sample absorbance between 1.8 and 2.1 were used for Real-time polymerase chain reaction (RT-PCR) analysis, then total RNA was converted into cDNA by Reverse Transcript kit MonScript™ RTIII All-in-One Mix with dsDNase (Wuhan, China). RT-PCR was carried out using TB Green® Premix Ex Taq™ II with CFX96 68 Touch System, and thermal cycling steps were programmed as 95 °C for 10 min, follow by 40 cycles of 95 °C for 10 s, 60 °C for 30 s, finally a melting curve was maintained at 95 °C for 15 s. RT-PCR was used to quantify expression of genes involved in Nrf2 signal pathway (Nrf2, keap-1, NQO-1, HO-1, hbeaf, gclc, gclm), endoplasmic reticulum stress (XBP1, CHOP, BIP, ATF4). The synthesis of primers for PCR amplification were obtained from Tsingke and primers are listed in Table S1. Glyceraldehyde-3-phosphate dehydrogenase (GAPDH) was used as an endogenous control to obtain relative quantitative values for gene expression.

RNA-sequence work was to extract cell RNA and delivered it to Meggie company for purification and sequencing. RNA sequence analysis was carried out by the online sequencing analysis platform provided by Meggie company. Next, Fastp software was used to assess the quality of raw sample data and RSEM can then be used to calculate gene or transcript expression through single- or dual-terminal sequencing data. Moreover, DESeq2 software based on negative binomial distribution was used to study differential expression of transcriptome samples. Finally, GO and KEGG databases were used for functional enrichment analysis of differential genes.

2.7. Statistical analysis

The values were expressed as means ± SD (n = 3), and the relative protein levels expressed as means ± SD were analyzed statistically with one-way ANOVA. Results from standard micronucleus assays were expressed as means and half-ranges of variation, and duplicate data were combined to become quantal data, followed by X^2 test. All experiments were replicated three times.

3. Results and discussion

As lack of relative research in TPHP in-vitro studies, it is of considerable significance to investigate long-term exposure cytotoxicity mechanism of TPHP to different respiratory tract cells from angle of whole respiratory tract. Herein, we mainly want to put forward the proof whether TPHP exposure induced cytotoxicity of top-down respiratory tract cells.

3.1. Toxicity caused by TPHP exposure

Cell viabilities of five different cells were firstly investigated upon exposed to TPHP with concentration ranging from 0 to 1000 μM under the identical condition. As Fig. 1 shows, for a given exposure time of 24 and 72 h, cell viabilities of all five different cells decreased gradually with increasing exposed TPHP concentration. Cells being less affected by TPHP at low concentrations might be because proliferation effect was greater than cell viability damage. Moreover, damage to cell viability with 72 h exposure was greater than 24 h exposure. Among these cell lines, cell viabilities of HNEpC and HFL1 cell lines were found to be mostly affected by TPHP. For HNEpC (Fig. 1a), cell viability decreased to 81.5% and 77.2% after exposure to 1000 μM TPHP for 24 and 72 h, respectively; while for HFL1 (Fig. 1e), cell viability dropped to 88.5% and 77.2%, respectively. In contrast, in the 72-h exposure group, activity of three other types of cells (16HBE, NP69 and Beas-2B) only decreased by 10.8%, 11.5% and 6.6% in the 1000 μM treatment group, respectively (Fig. 1b-d). These results indicate that HNEpC and HFL1 cells were the two types of the cells most affected by TPHP.

These results were double confirmed by LDH test as shown in Fig. S1. That is, during 72 h exposure time, the two most sensitive cell lines (HNEpC and HFL1) also had the severest release of LDH during TPHP exposure, reached approximately 240.9 and 313.2 U/L in 1000 μM exposure group. LDH level of 16HBE was below 100 U/L at all TPHP concentrations (Fig. S1b), indicating that no rupture of all these five kinds cells occurred under such exposure conditions.

Furthermore, stress levels of all studied five different cells were compared after injury by TPHP exposure. As Fig. 2 shows, the change trends of intracellular ROS levels in 72 h exposure mode were consistent with the cell damage viability tests (Fig. 1), so subsequent experiments were all carried out over 72 h duration. To be specific, 100 μM TPHP exposure for 72 h could enhance to 1.4 and 0.9 for HNEpC and HFL1 cells, respectively (Fig. 2a and e), as compared with other three cells (16HBE, NP69 and Beas-2B) obtained as 0.7, 0.6 and 0.7 (FL/FL_0), respectively. These results indicate that TPHP exposure could extremely lead to stress of both HNEpC and HFL1 cells and produce higher ROSs.

The induction of ROSs in cells can subsequently produce various antioxidant enzymes (He et al., 2017; Morry et al., 2017; Rajendran et al., 2014). Thus, activities of a series of antioxidant enzymes including CAT and SOD were assayed in five different respiratory tract cells upon exposed to TPHP for 72 h. As Fig. 3a and b shows, the activities of CAT and SOD in HNEpC cells significantly induced to 42.9 and 223.1 U/mg protein at 100 μM TPHP, respectively. SOD and CAT concentration in 16HBE, NP-69, Beas-2B cells were all within 100 U/mg protein. However, inconsistent with above obtained results, the production levels in both antioxidant enzymes in HFL1 cells were not obvious, which may be due to that HFL1 cells do not produce antioxidant enzymes to remove the generated intracellular ROSs. So, detoxification of glutathione should be considered.

To further study genotoxicity effects of TPHP exposure on different respiratory tract cells, micronucleus formation was also assayed, which can reflect chromosome breakage and loss of whole chromosome including clastogenicity and aneugenicity of subject matter (Fenech et al., 2011; McLaughlin et al., 2020; Reisz et al., 2014). Herein, as Fig. S2 shows, TPHP induced micronucleus formation in HNEpC and HFL1 cells at relatively low TPHP concentration (1 μM) with a concentration dependence manner. Specifically, micronucleus formation in HNEpC cells was more pronounced with 38 and 45 micronuclei per 1000 cells under stimulation of 1 and 100 μM TPHP, respectively. Comparatively, micronuclei number in HFL1 cells increased steadily with exposure, reaching 38 micronuclei per 1000 cells for 100 μM TPHP exposure. In contrast, TPHP only induced 16HBE, Beas-2B and NP69 cells to produce micronucleus at much higher concentration than 10 μM. In all, more micronucleus formation was induced in HNEpC and HFL1 cells than other cells, which was consistent with our above obtained results. However, when the inhibitor ABT or NAC was added into TPHP

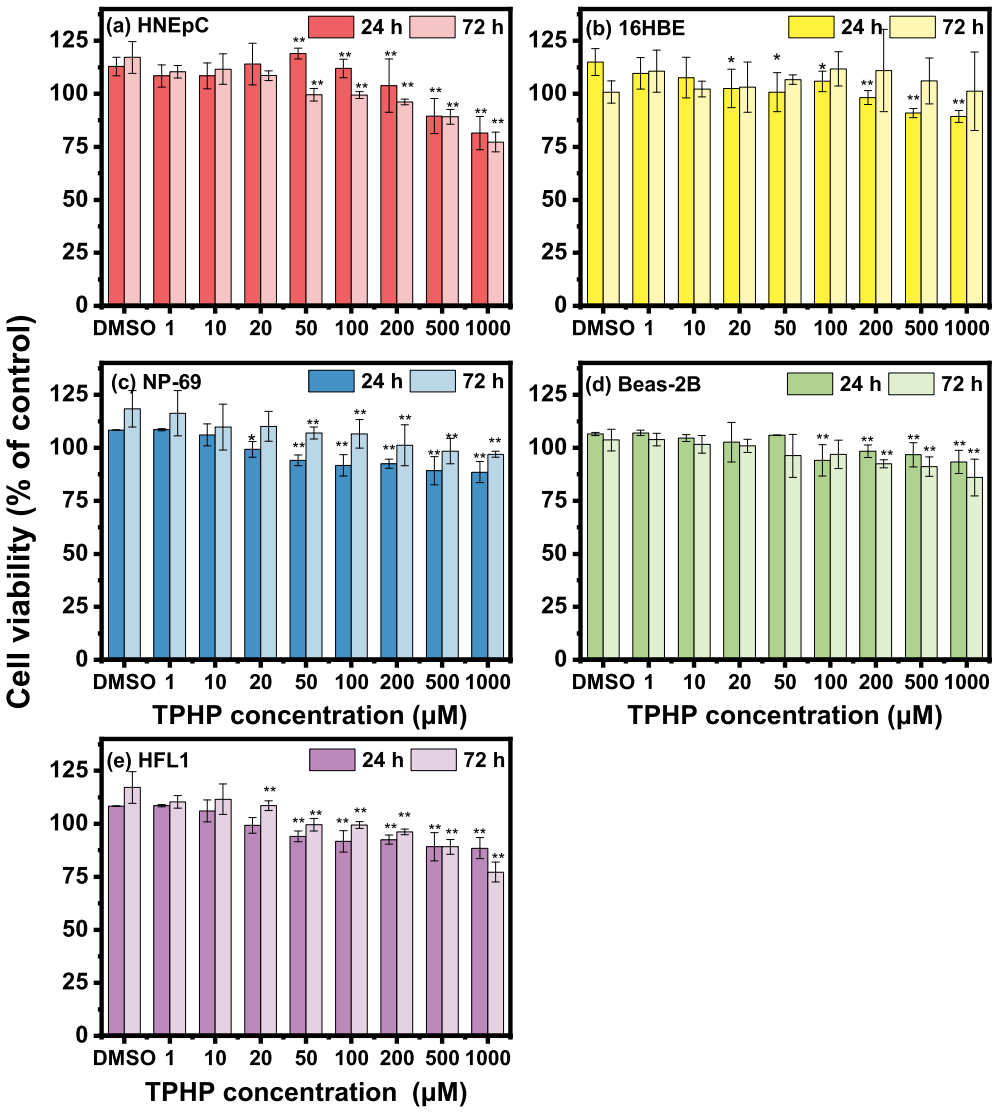

Fig. 1. Cell viability assay of five respiratory tract cells upon exposed to TPHP for 24 and 72 h. (a) HNEpC, (b) 16HBE, (c) NP-69, (d) Beas-2B, (e) HFL1. DMSO group was used as solvent control. Each histogram represents mean ± S.D. of three experiments done in triplicate. $*p < 0.05$, $**p < 0.01$ versus control.

exposure groups, micronucleus formation was significantly inhibited, further confirming that TPHP exposure can really induce chromosome breakage or even the loss of whole chromosome for all five kinds cells especially for HNEpC and HFL1 cells.

3.2. *The role of endoplasmic reticulum (ER) stress in the early stress response*

ER is an organelle with many functions. Many early conditions stress in cells, including starvation, hypoxia, infection, and changes in secretory needs that challenge the folding capacity of cells and enhance ER stress (Iurlaro and Munoz-Pinedo, 2016; Phillips and Voeltz, 2016; Wang and Kaufman, 2016). In this study, high exposure group (100 μM) of TPHP significantly induced ER stress-related genes including ATF4 (activating transcription factor), BIP (glucose regulated protein), CHOP (proapoptotic factor C/EBP Homologous protein), and XBPI (X-box bBinding protein 1), and increased by 17.0, 10.8, 79.1, 44.4 folds in HNEpC cells as compared with the control group, respectively (Fig. 4). The following is HFL1 cells (Fig. 4e), in which these genes were upregulated 2.7, 5.7, 23.5 and 2.8 times compared with blank group, respectively. For three other types of cells, these genes were regulated from 0.2 to 12.4 times, which is not obvious compare with HNEpC and HFL1 cells (Fig. 4c). This result can be echoed with the result that HFL1 and HNEpC were most severely damaged by TPHP as shown in Fig. 1. These results indicate that all respiratory tract cells especially HNEpC and HFL1 cells initiated early self-rescue mechanism prominently after TPHP exposure.

Generally, when ER stress fails to restore normal cell function, mitochondria - induced apoptosis pathways will be activated, by inducing Ca^{2+} production in cytoplasm (Demidchik et al., 2018; Giorgi et al., 2018; Jacob et al., 2021; Rizzuto et al., 2012). Therefore, Ca^{2+} concentrations in cytoplasm of five different cells were measured to see if cells could save themselves by initiating Ca^{2+}-induced mitochondrial pathways. As Fig. 5 shows, the intracellular Ca^{2+} levels in 16HBE, NP69 and Beas-2B cells were significantly affected by TPHP exposure, and increased by 1.7, 1.1 and 1.3 times, respectively, as compared with the control. However, TPHP did not caused a significant increase in Ca^{2+} of the other two cell lines (HNEpC and HFL1). These results suggest that HNEpC and HFL1 cells were irretrievably damaged by ER stress in short-term exposure system, and did not initiate stress induction in later Ca^{2+}-mitochondrial pathway.

Further, it has been reported that when the ER induced changes in Ca^{2+} content fail to maintain body homeostasis due to differences in time and intensity of stimulation in various cells. Cells will experience

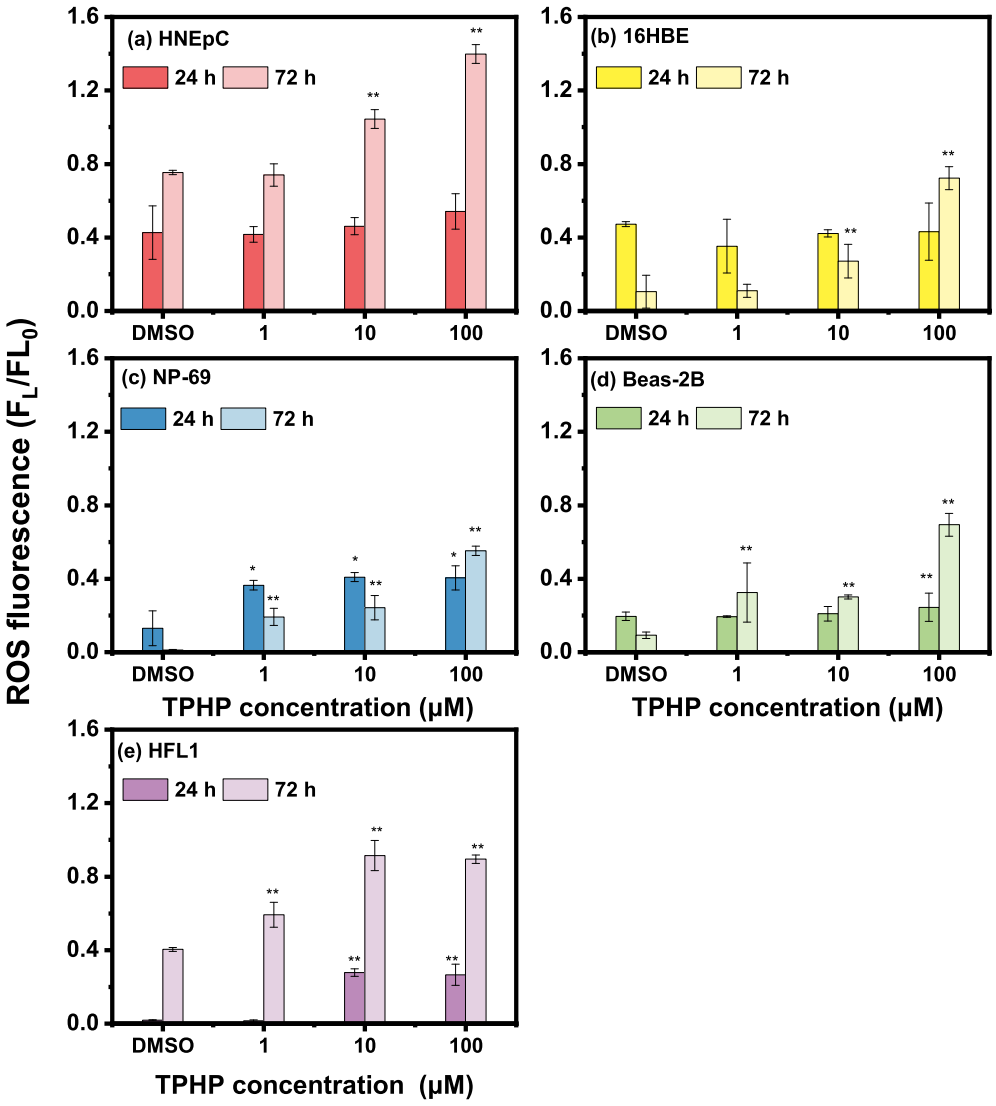

Fig. 2. ROS induction of five different respiratory tract cells upon exposed to TPHP for 24 and 72 h. (a) HNEpC, (b) 16HBE, (c) NP-69, (d) Beas-2B, (e) HFL1. DMSO group was used as solvent control. Each histogram represents mean ± S.D. of three experiments done in triplicate. $^*p < 0.05$, $^{**}p < 0.01$ versus control.

irreversible mitochondria-induced apoptosis to clear the damaged cells (Hetz, 2012; Woehlbier and Hetz, 2011). With prolonging exposure time, toxic damage to cells could reach mitochondria. Then, mitochondrial membrane potential (ΔΨm) was measured at the injured end (Twig and Shirihai, 2011; Zorova et al., 2018), which can be characterized by a shrinkage in fluorescence intensity ratio of JC-1 polymer/monomer (Fig. S3). As Fig. 6 shows, Δψm level had a downward trend with increasing TPHP concentrations for all investigated cell lines. Specifically, Δψm level in HFL1 and HNEpC cells showed 0.6 and 0.6 times downward as compared with the control, while 16HBE, Beas-2B and NP69 cells presented a sluggish sagging tendency of 1.1, 0.7, 0.8 times, respectively. Based on the above data, it can be concluded that not only at the early stage (ER), but also at the late stage (mitochondria), both HFL1 and HNEpC cells were severely destructed, which is irreversible. In contrast, 16HBE, Beas-2B and NP69 cell could initiate rescue mechanism at the early ER stress stage after TPHP exposure, during which Ca^{2+} outflow was obvious, and short-term self-repair was realized, then decreasing trend of terminal MMP was alleviated. Likewise, similar phenomenon was reported previously (Hetz, 2012; Oyadomari and Mori, 2004).

3.3. *Nrf2 signaling pathway mediated detoxification*

As mentioned above, some cells like HFL1 cells may not produce the CAT and SOD to eliminate free radicals, and they may use their glutathione detoxification system to serve similar function (Lu, 2013; Yang et al., 2005). Therefore, Nrf2 signaling pathway and downstream glutathione detoxification system were also measured. Literatures showed that the concentration of FBS in cells has an impact on gene expression in cells. To control variables and ensure that cells are tested in a healthy environment, we used different concentrations of FBS to carry out excretion interference experiments against Beas-2B cells. As Fig. S4 shows, the addition of FBS to TPHP exposure system had little effect on cell gene expression.

The expressions of genes related to the Nrf2 pathway was firstly investigated (Fig. 4). TPHP induced the expressions of Nrf2 (nuclear erythroid 2-related factor), Keap-1 (Kelch-1 ike ECH-associated protein l) and NQO-1(NAD(P)H:quinone oxidoreductase 1) genes in HNEpC cells up-regulated by 1.3–2.8, 1.1–1.2 and 2.7–7.0 times, respectively. However, in Beas-2B cells, these genes were regulated to 0.3–1.7, 0.2–0.5 and 0.1–1.2 of the control group, showing the weakest effect of Nrf2 on regulation. In addition, other genes including gclc (glutamate-cysteine ligase catalytic), gclm (glutamate-cysteine ligase modifier)

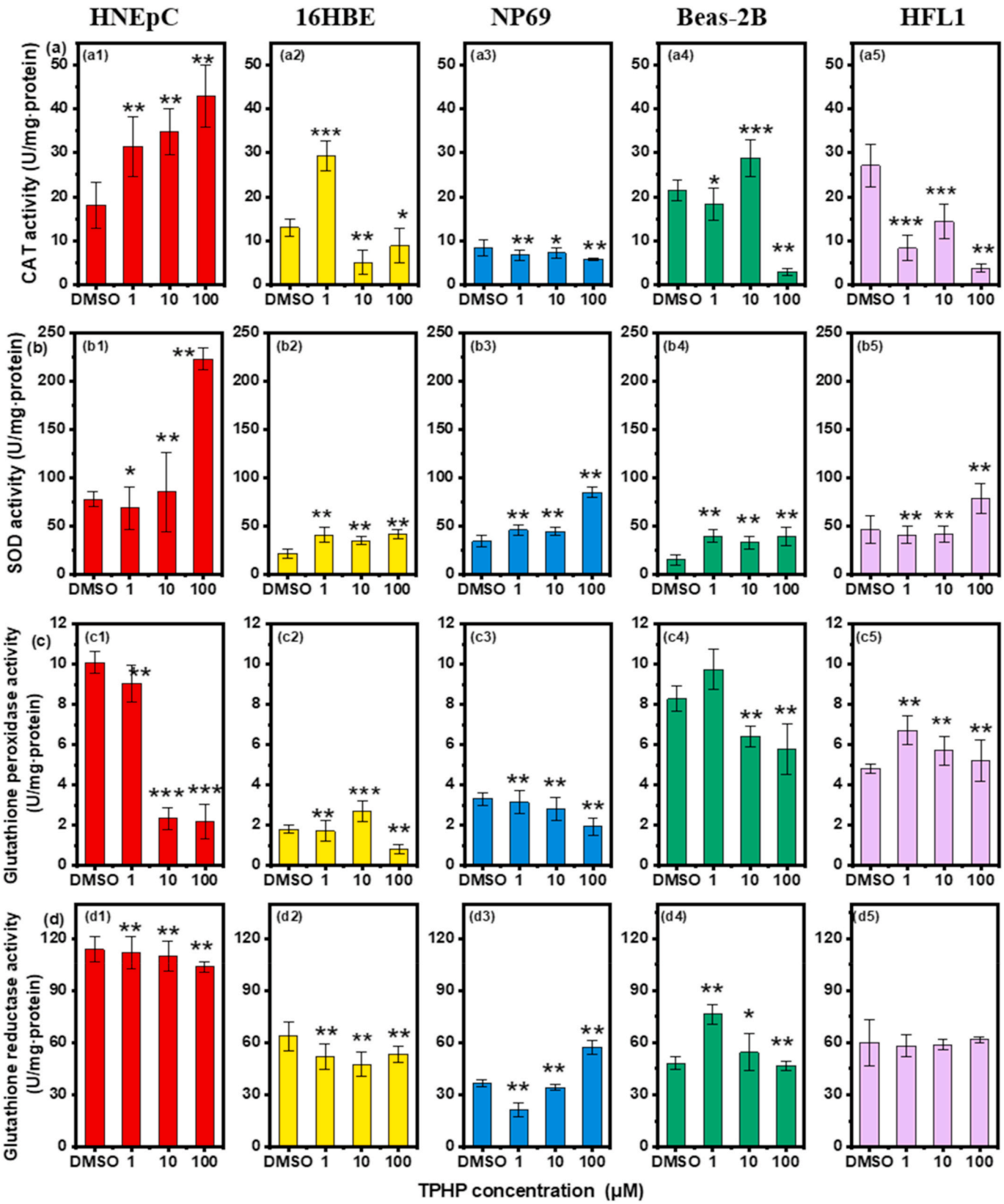

Fig. 3. CAT activity (a1 – a5), SOD activity (b1 – b5), GSH-Px activity (c1 – c5), and GR activity (d1 – d5) of five different respiratory tract cells upon exposed to TPHP for 72 h. DMSO group was used as solvent control. Each histogram represents mean ± S.D. of three experiments done in triplicate. *$p < 0.05$, **$p < 0.01$ versus control.

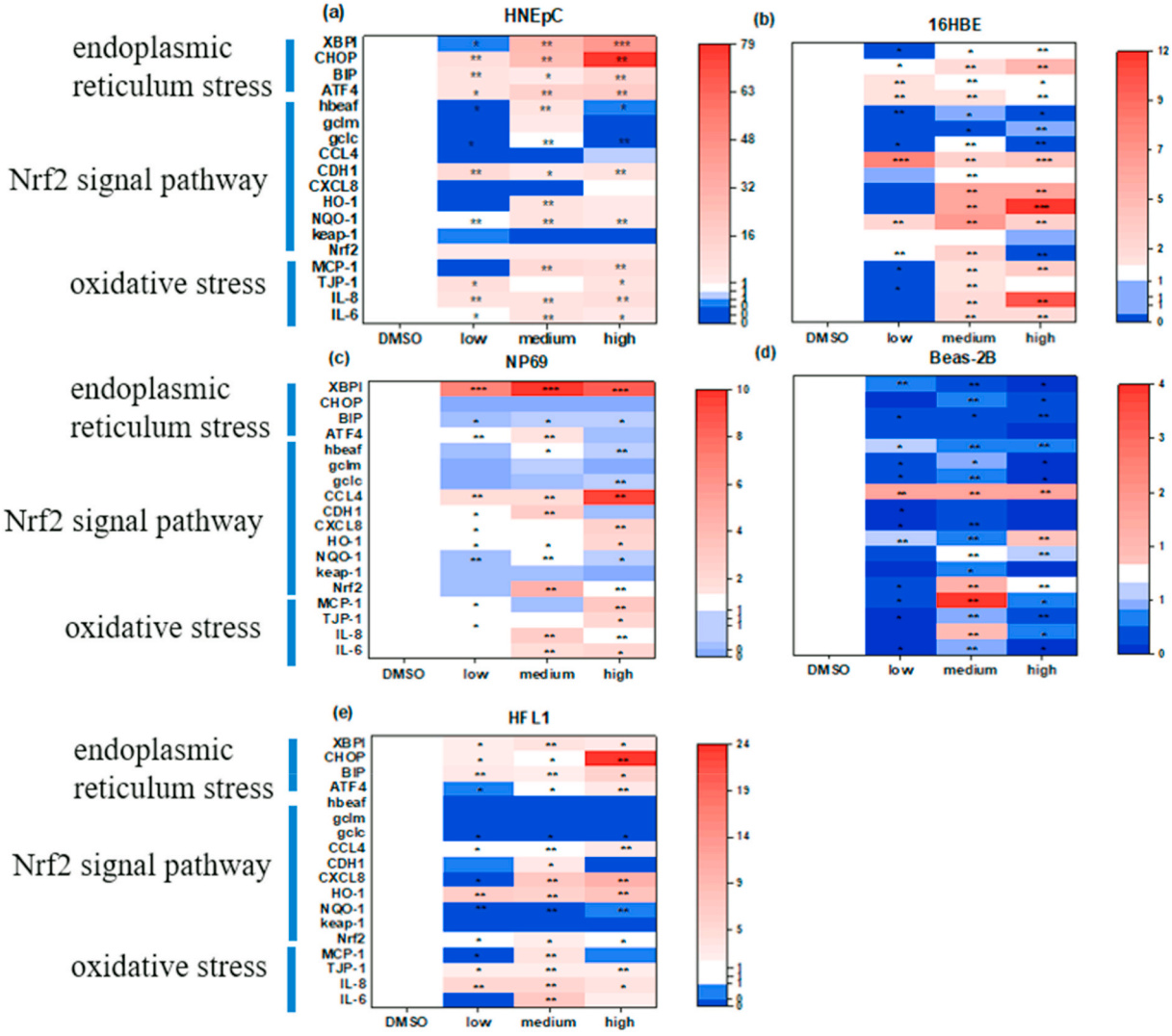

Fig. 4. Comparison of TPHP (1, 10, 100 μM, 72 h) mediated endoplasmic reticulum stress, oxidative stress, Nrf2 pathway related gene alteration. For (a) HNEpC, (b) 16HBE, (c) NP-69, (d) Beas-2B, (e) HFL1. 0 was used as blank control, and DMSO group was used as solvent control. Low, medium and high concentrations correspond to TPHP of 1, 10 and 100 μM, respectively. Each histogram represents mean ± S.D. of three experiments done in triplicate. *$p < 0.05$, **$p < 0.01$ versus control.

genes were also regulated by Nrf2 signal pathway (Lu, 2013). In this study, all these genes were found to be inhibited to various degrees in the tested cell lines. For example, they were inhibited by 0.3–1.4, 0.1–0.7 times, respectively, to the control in HNEpC cells (Fig. 4), which is the most regulated the tested cell lines. Following is in HFL1 cells, which down-regulated around 0–0.1, 0–0.1 times to the control, respectively. Confirming our previous conjecture that HFL1 cells remove intracellular ROSs through glutathione detoxification rather than production of antioxidant reactive kinase. Levels of gclc and gclm in different cells slightly down-regulated (Fig. 4), indicating that TPHP could induce activation of detoxification system via the Nrf2 pathway to some extent.

Further, enzyme activities of glutathione detoxification system were tested. As reported, the oxidized glutathione (GSSG) is reduced to glutathione (GSH) in a NADPH-dependent manner by reducing glutathione reductase 1 (GSR1) (Kim et al., 2012), which is another target of Nrf2. By synergistically activating GSH generation, utilization, and regeneration, Nrf2 reduced intracellular GSH levels are maintained (Niture et al., 2014; Taguchi and Yamamoto, 2017). Therefore, GSH-Px activities in these studied cell lines were also evaluated when exposed to TPHP. As Fig. 3c illustrates, for NP69 and HFL1 cells, each concentration of TPHP had little effect on GSH-Px activity. In contrast, GSH-Px activity in Beas-2B and 16HBE cells increased to 9.7, and 6.7 U/mg·protein, respectively, after 1 μM TPHP exposure. Whereas, GSH-Px activity in HNEpC cells decreased significantly from 4.1 to 1.6 U/mg protein under 72 h exposure. These results point out that HNEpC cells can recover to redox stasis by activating glutathione detoxification system and degrading oxygen free radicals *in vivo*. In addition, these results were consistent with our above obtained findings, that is, HNEpC cells consistently faced the greatest impact.

In addition, previous study has displayed that slacken GR can deplete GSH and bring about upregulation of intracellular ROSs (Kim et al., 2010). In this study, GR levels in Beas-2B, 16HBE and HFL1 cells did not fluctuate significantly after exposure of TPHP (Fig. 3d). GR activity in NP69 cells increased to 57.3 U/mg·protein after 100 μM TPHP exposure. In contrast, GR activity in HNEpC cells decreased dramatically from 113.8 U/mg·protein in the control group to 103.7 U/mg·protein in 100 μM TPHP. Overall, HNEpC regulated Nrf2 downstream genes to control GSH detoxification levels to achieve homeostasis more obviously than the other.

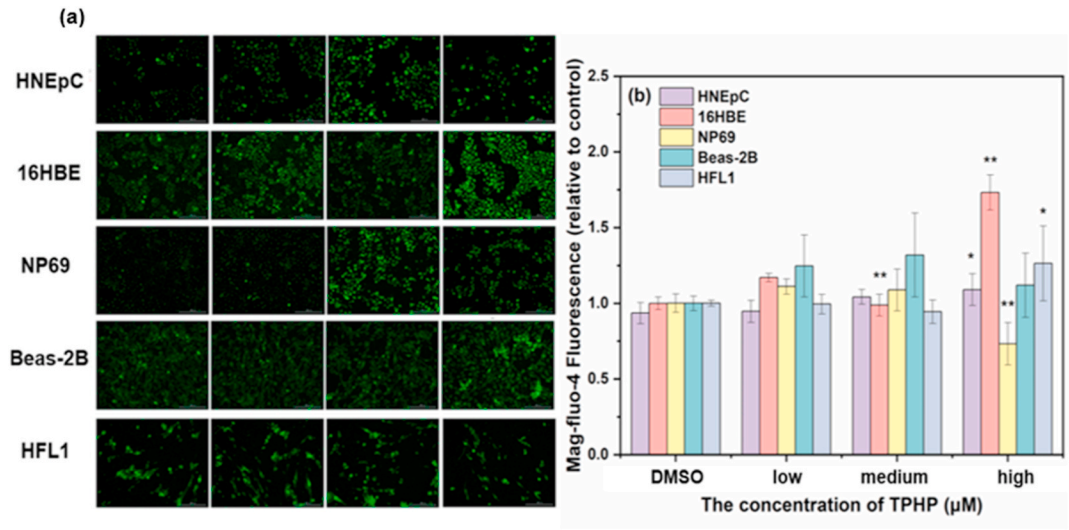

Fig. 5. Intracellular Ca^{2+} levels in five different cells after 72 h of TPHP exposure (1, 100 μM). (a) for HNEpC, 16HBE, NP-69, Beas-2B, HFL1; (b) Comparison of fluorescence intensity of Ca^{2+} in five kinds of cells. Cytoplasmic Ca^{2+} was labeled with Fluo-4 (green), and one of typical image was exhibited. Bars represent mean ± SD, n = 5. * shows the significant difference, $P < 0.05$. (For interpretation of the references to colour in this figure legend, the reader is referred to the Web version of this article.)

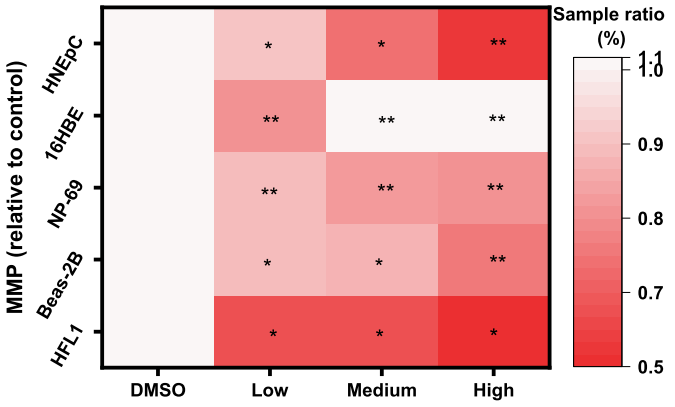

Fig. 6. Fluorescence microscopy of ΔΨm in five different cells after 72 h of TPHP exposure (1, 10, 100 μM). Heat map shows fluorescence intensity for different cells. The fluorescence intensity of JC-1 aggregates and JC-1 monomers in mitochondria were measured by laser confocal microscope.

3.4. Detection of disease-related cytokines corresponding

To determine whether TPHP has different pathological effects on various respiratory cells, cytokine/chemokine tests were performed on cells for their corresponding diseases.

As the first physical barrier against pollutants, viruses and bacteria, HNEpC play an important role in pre-immunization and preventive immunization (Nian et al., 2020; Yu et al., 2017). VEGF is the most important driving factor of vascular formation. Excessive production of VEGF not only promotes mucosal edema, but also promotes antigen sensitization and type 2 helper T cell-related inflammation (Kwak et al., 2020; Matsune et al., 2008). In present work, VEGF levels of HNEpC were determined to characterize the influence of TPHP on the pathogenesis of chronic sinusitis in HNEpC (Fig. S5a). VEGF content increased from 759.9 to 3278.3 ng/mL, when TPHP concentration increased from 1 to 100 μM. This indicates that TPHP exposure may induce a certain level of inflammatory response.

Matrix metalloproteinase (MMPs) are involved in remodeling the extracellular matrix and several members of this family are involved in pulmonary epithelial repair mechanisms (Vandooren et al., 2013; Yabluchanskiy et al., 2013). Among these members, MMP-9 is a key marker for chronic obstructive pulmonary disease (COPD) (Chaudhuri et al., 2013). In this study, MMP-9 level in 16HBE cells were slowly rising from 1 μM to 4.3 μg/mL and then up to 10.6 μg/mL (Fig. S5b). This result indicates that 16HBE cells exposed to TPHP induced *in vivo* activation of epithelial repair MMP-9 enzymes, initiating epithelial repair mechanisms.

Activation of tumor necrosis factor alpha (TNF-α) is an important factor in the canceration of NP69 to nasopharyngeal carcinoma cells (Awasthi et al., 2008; Kim et al., 2018). In this study, it was found that TNF-α content was not dose-dependent with TPHP concentration (Fig. S5c), demonstrating that TPHP exposure has no obvious effect on human throat cell carcinogenesis.

Airway epithelial cells not only act as a protective barrier to external environment, but also can initiate and amplify airway inflammation through producing a variety of pro-inflammatory mediators, including GM-CSF, which is typically significantly elevated in epithelial cells of asthmatic patients (Adkins et al., 1998; Marini et al., 1991; Zhao et al., 2020). In this study, after exposure to TPHP, GM-CSF concentration in Beas-2B cells gradually increased from 348.0 pg/mL in 1 μM–477.2 pg/mL in 100 μM (Fig. S5d), indicating that TPHP has a certain influence on the inflammatory initiation of lung epithelial cells.

Transforming growth factor β1 (TGF-β1) is one of the important factors that promote myofibroblast differentiation (Hao et al., 2019). As Fig. S5e shows, TGF-β1 changes were not significant in HFL1 cells after TPHP exposure, ranging from 19.9 to 22.6 ng/mL. These results indicate that TPHP could hardly induce HFL1 cells to differentiate from fibroblasts to myofibroblasts at 1–100 μM.

Overall, it can be found that TPHP affects inflammatory response of nose and immune system and is associated with sinusitis.

3.5. Effect of TPHP-induced gene sequence in HNEpC cells

Based on the above obtained results, we can find that HNEpC cells were the mostly affected by TPHP exposure. In order to further analyze the mechanism of TPHP exposure to HNEpC cells, RNA sequencing was performed. Six groups of experiments were carried out as follows: the control group, solvent control group, 1, 10, 100, and 1000 μM TPHP based on HNEpC cells cultured with only medium, medium with DMSO, medium with 1, 10, 100, 1000 μM TPHP, respectively. The principal component analysis (PCA) demonstrated that a certain distance of

similarity existed between the six groups of experiments (Fig. S6a). Among them, the 100 and 1000 μM TPHP exposure groups differed significantly from the other four groups. Therefore, it was believed that TPHP significantly influence the gene expression in HNEpC cells. In addition, the overall gene expression level of all samples was about 1 (Fig. S6b), which was relatively stable. Based on the correlation analysis from Fig. S6c, it was found that there was a substantial correlation between the blank control, the solvent control and two low concentration exposure groups, as well as between the two medium and high concentration exposure groups. These results indicate that TPHP exposure dose has a certain relationship with modification of gene expression in HNEpC cells, which also proves the effectiveness of experimental design.

Next, Venn analysis of RNA-Seq by Expectation Maximization (RSEM) (Fig. S7a) was also used to screen genes with expression level above 10, and it was found that 6137 genes were co-expressed in six different treatment groups. We analyzed differential gene sets (Fig. S7b and S7c) and established in pairs between the solvent control and the four exposed groups, which we call them differentially expressed genes (DEGs). In the 1 and 1000 μM TPHP treatment groups, 2392 genes up-regulated, 2266 genes down-regulated, and total number of differentially expressed genes was 4658, which has the largest number of DEGs. In addition, 1768 genes up-regulated and 1986 genes down-regulated in DMSO group and 1000 μM TPHP group, and total number of DEGs was 3754. Overall, the effect of TPHP exposure on HNEpC cell gene expression increased with the maximum dose.

To further analyze concentration-dependent effect of TPHP on HNEpC cells, DEGs of three groups of 1, 100, and 1000 μM were selected for pair analysis. Based on GO classification statistical results (Fig. 7a), process involving cell process (multicellular organisms process, biological control, reproductive process, movement process, the breeding process of stimulus-response, biofouling, positioning, immune system, metabolic process, number of proliferation, growth, cell membrane, organelle, compound protein connections, and synapses), cell and molecular biological process (transport activity, molecules, CAT activity, molecular function regulation, molecular transfer activity, and transcriptional regulation activity) were fundamentally regulated. Furthermore, based on the analysis of GO database for 1 and 1000 μM DEG (Fig. 7c), it was found that some genes involved epithelial cell growth, migration, migration of endothelial cells, wound healing, histone acetylation, endoplasmic reticulum stress, white blood cells apoptosis, myelination, epidermal growth factor receptor signaling pathway, protein kinase B signaling pathway is widely regulated. Similarly, KEGG enrichment pathway analysis (Fig. 7b) for above gene sets showed that MAPK signaling pathway, cytokine-cytokine receptor interaction, VEGF

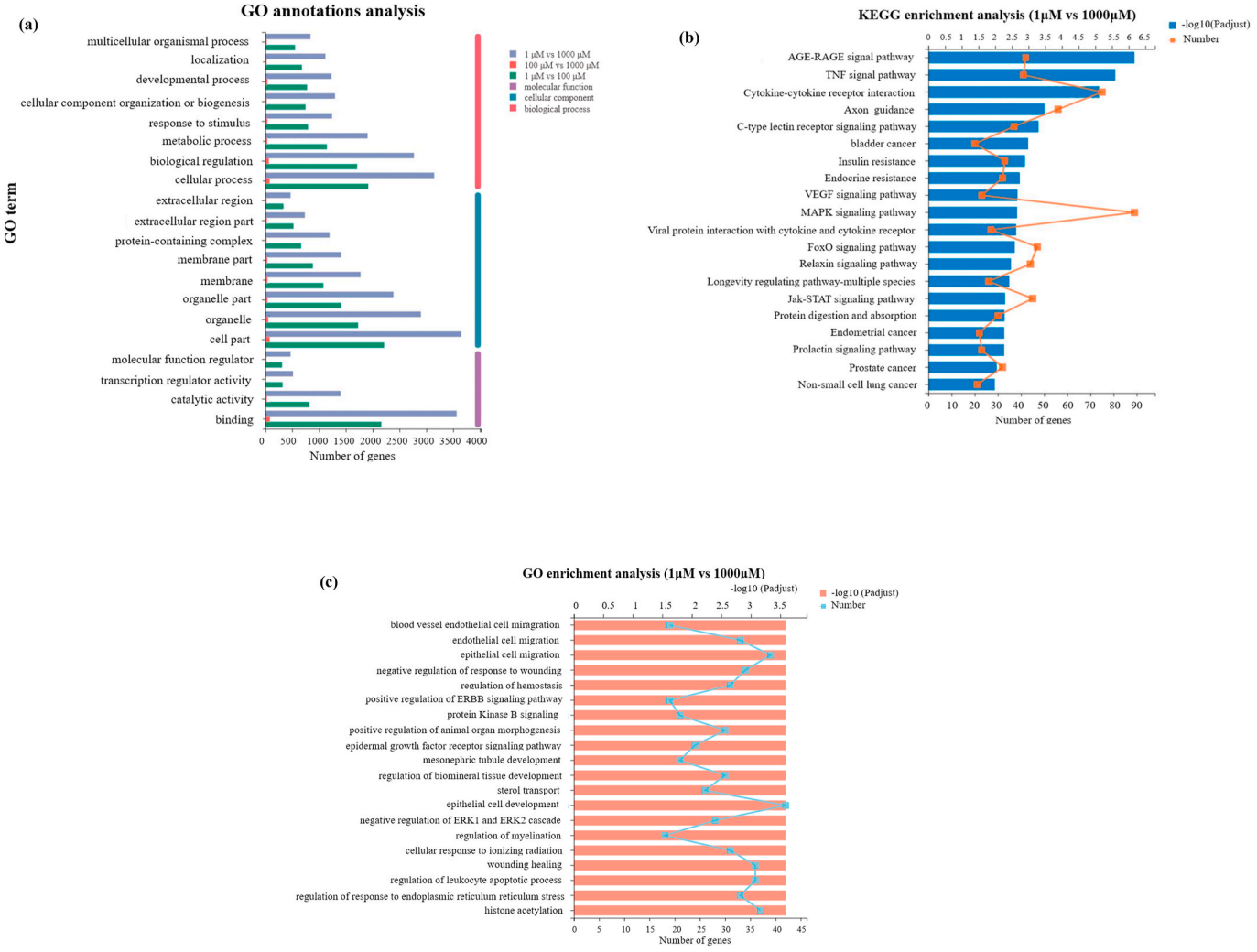

Fig. 7. Bioinformatics analysis of gene expression after TPHP exposure to HNEpC. Principal component analysis (PCA) analysis (a) shows similarity between samples, and distance between samples reflects the size of the correlation between samples. The increase of the distance between samples indicates that there is a significant difference between samples; (b) Analysis of correlation results between samples. Heat map reflects correlation between samples. The closer correlation coefficient is to 1, the greater correlation will be; (c) display GO annotation analysis between different treatment group and (d) show KEGG enrichment analysis between 1 and 1000 μM treatment group.

signaling pathway (according to the above description, the level of VEGF in HNEpC cells exposed to TPHP was measured, and the level of VEGF increased from 759.9 to 3278.3 ng/mL (Fig. S5a)), protein digestion and absorption, JAK-STAT signaling pathway, laxin signaling pathway, FoxO signaling pathway and C-type lectin receptor signaling pathway were also significantly altered.

4. Conclusion

In conclusion, oxidative stress, ER stress levels and corresponding pathological-related factors/chemokines were compared and evaluated under top-down exposure of different concentrations of TPHP to five different types of respiratory tract cells. The results indicate that HNEpC cells were the most severely damaged, ROS level increased, and anti-oxidant kinases, including CAT, SOD, GR, GSH-Px, and gene expression levels increase most significantly under 72 h exposure to TPHP. We also demonstrated that the response of HNEpC cells is the most obvious in the Nrf2 detoxification pathway.

On that occasion, it was surprised to find that both the early stage (ER) and the late stage (mitochondria) of HFL1 and HNEpC cells were serious injury, which showed irreversible changes. It was speculated that 16HBE, Beas-2B, and NP69 were activated by the early-stage ER stress rescue mechanism after the exposure, and Ca^{2+} outflow was obvious, which realized short-term self-repair, and the decline trend of terminal MMP was alleviated. RNA-sequence results suggests that the increase of VEGF after TPHP exposure aggravates HNEpC cells' chronic sinusitis and destroys the airway epithelial barrier function, leading to the destruction of airway immune tolerance. In the end, KEGG enrichment analysis showed that VEGF and MAPK signaling pathway was regulated to a certain extent in HNEpC cells. These findings will help to understand the relationship between TPHP on HNEpC pathological factor production and molecular mechanism regulation of cell genes, and help to further reveal the influence of TPHP on pathogenesis and signaling of chronic sinusitis.

Credit author statement

Jingyi Chen: Methodology, Formal analysis, Writing – original draft. **Guiying Li**: Writing – review & editing, Supervision. **Hang Yu**: Visualization, Investigation. **Hongli Liu**: Methodology, Formal analysis. **Taicheng An**: Conceptualization, Supervision.

Declaration of competing interest

The authors declare that they have no known competing financial interests or personal relationships that could have appeared to influence the work reported in this paper.

Acknowledgements

This work was supported by the National Key Research and Development Project (2019YFC1804504 and 2019YFC1804503), National Natural Science Foundation of China (41731279, 41991314 and 41877363), and Local Innovative and Research Teams Project of Guangdong Pearl River Talents Program (2017BT01Z032).

Appendix A. Supplementary data

Supplementary data to this article can be found online at https://doi.org/10.1016/j.envpol.2022.119564.

References

Adkins, K.K., Levan, T.D., Miesfeld, R.L., Bloom, J.W., 1998. Glucocorticoid regulation of GM-CSF: evidence for transcriptional mechanisms in airway epithelial cells. Am. J. Physiol. 275, L372–L378.

Al-Salem, A.M., Saquib, Q., Siddiqui, M.A., Ahmad, J., Wahab, R., Al-Khedhairy, A.A., 2019. Organophosphorus flame retardant (tricresyl phosphate) trigger apoptosis in HepG2 cells: transcriptomic evidence on activation of human cancer pathways. Chemosphere 237, 124519.

Araki, A., Saito, I., Kanazawa, A., Morimoto, K., Nakayama, K., Shibata, E., Tanaka, M., Takigawa, T., Yoshimura, T., Chikara, H., Saijo, Y., Kishi, R., 2014. Phosphorus flame retardants in indoor dust and their relation to asthma and allergies of inhabitants. Indoor Air 24, 3–15.

Awasthi, G., Singh, S., Dash, A.P., Das, A., 2008. Genetic characterization and evolutionary inference of TNF-alpha through computational analysis. Braz. J. Infect. Dis. 12, 374–379.

Basaran, B., Civan, M.Y., 2021. Investigating of primary components and source apportionment of persistent organic pollutants of indoor dust. Int. J. Environ. Sci. Technol. 18, 2145–2160.

Björnsdotter, M.K., Romera-García, E., Borrull, J., de Boer, J., Rubio, S., Ballesteros-Gómez, A., 2018. Presence of diphenyl phosphate and aryl-phosphate flame retardants in indoor dust from different microenvironments in Spain and The Netherlands and estimation of human exposure. Environ. Int. 112, 59–67.

Cao, Z., Zhao, L., Zhang, Y., Ren, M., Zhang, Y., Liu, X., Jie, J., Wang, Z., Li, C., Shen, M., Bu, Q., 2019. Influence of air pollution on inhalation and dermal exposure of human to organophosphate flame retardants: a case study during a prolonged haze episode. Environ. Sci. Technol. 53, 3880–3887.

Chaudhuri, R., McSharry, C., Spears, M., Brady, J., Grierson, C., Messow, C.M., Miele, G., Nocka, K., MacNee, W., Connell, M., Murchison, J.T., Sproule, M., Hilmi, O., Miller, D.K., Thomson, N.C., 2013. Sputum matrix metalloproteinase-9 is associated with the degree of emphysema on computed tomography in COPD. Transl. Respir. Med. 1, 11.

Demidchik, V., Shabala, S., Isayenkov, S., Cuin, T.A., Pottosin, I., 2018. Calcium transport across plant membranes: mechanisms and functions. New Phytol. 220, 49–69.

Dodson, R.E., Perovich, L.J., Covaci, A., Van den Eede, N., Ionas, A.C., Dirtu, A.C., Brody, J.G., Rudel, R.A., 2012. After the PBDE phase-out: a broad suite of flame retardants in repeat house dust samples from California. Environ. Sci. Technol. 46, 13056–13066.

Estill, C.F., Mayer, A., Slone, J., Chen, I.C., Zhou, M., La Guardia, M.J., Jayatilaka, N., Ospina, M., Calafat, A., 2021. Assessment of triphenyl phosphate (TPhP) exposure to nail salon workers by air, hand wipe, and urine analysis. Int. J. Hyg Environ. Health 231, 113630.

Fenech, M., Kirsch-Volders, M., Natarajan, A.T., Surralles, J., Crott, J.W., Parry, J., Norppa, H., Eastmond, D.A., Tucker, J.D., Thomas, P., 2011. Molecular mechanisms of micronucleus, nucleoplasmic bridge and nuclear bud formation in mammalian and human cells. Mutagenesis 26, 125–132.

Giorgi, C., Marchi, S., Pinton, P., 2018. The machineries, regulation and cellular functions of mitochondrial calcium. Nat. Rev. Mol. Cell Biol. 19, 713–730.

Hanas, A.K., Guigueno, M.F., Fernie, K.J., Letcher, R.J., Chamberland, F.S.M., Head, J.A., 2020. Assessment of the effects of early life exposure to triphenyl phosphate on fear, boldness, aggression, and activity in Japanese quail (*Coturnix japonica*) chicks. Environ. Pollut. 258, 113695.

Hao, Y., Baker, D., ten Dijke, P., 2019. TGF-β-mediated epithelial-mesenchymal transition and cancer metastasis. Int. J. Mol. Sci. 20, 2767.

He, L., He, T., Farrar, S., Ji, L.B., Liu, T.Y., Ma, X., 2017. Antioxidants maintain cellular redox homeostasis by elimination of reactive oxygen species. Cell. Physiol. Biochem. 44, 532–553.

Hetz, C., 2012. The unfolded protein response: controlling cell fate decisions under ER stress and beyond. Nat. Rev. Mol. Cell Biol. 13, 89–102.

Hong, X.S., Chen, R., Hou, R., Yuan, L.L., Zha, J.M., 2018. Triphenyl phosphate (TPHP)-induced neurotoxicity in adult male Chinese rare minnows (Gobiocypris rarus). Environ. Sci. Technol. 52, 11895–11903.

Iurlaro, R., Munoz-Pinedo, C., 2016. Cell death induced by endoplasmic reticulum stress. FEBS J. 283, 2640–2652.

Jacob, P., Kim, N.H., Wu, F.H., El Kasmr, F., Chi, Y., Walton, W.G., Furzer, O.J., Lietzan, A.D., Sunil, S., Kempthorn, K., Redinbo, M.R., Pei, Z.M., Wan, L., Dangl, J.L., 2021. Plant "helper" immune receptors are Ca^{2+}-permeable nonselective cation channels. Science 373, 420–425.

Ji, Y.B., Gao, S.Y., Ji, C.F., Zou, X., Yu, L., 2008. The Effect of Solanine on the Membrane Potential of Mitochondria in HepG2 Cells and $[Ca^{2+}]i$ in Cells. International Seminar on Future BioMedical Information Engineering, pp. 329–332.

Kempermann, G., 2019. Environmental enrichment, new neurons and the neurobiology of individuality. Nat. Rev. Neurosci. 20, 235–245.

Kim, J.S., Han, J.H., Seo, J., Lim, J.S., Jung, C., Park, I.S., Kang, H.R., Kim, S.S., Kim, H. J., Yoon, J.H.P., 2012. Alteration of GSSG/GSH ratio modulates expression of phase 2 detoxifying enzymes through Nrf2 signaling pathway. FEBS J. 26, 1.

Kim, M., Jung, K., Kim, I.-S., Lee, I.-S., Ko, Y., Shin, J.E., Park, K.I., 2018. TNF-alpha induces human neural progenitor cell survival after oxygen-glucose deprivation by activating the NF-kappaB pathway. Exp. Mol. Med. 50, 1–14.

Kim, S.J., Jung, H.J., Hyun, D.H., Park, E.H., Kim, Y.M., Lim, C.J., 2010. Glutathione reductase plays an anti-apoptotic role against oxidative stress in human hepatoma cells. Biochimie 92, 927–932.

Kwak, S., Choi, Y.S., Na, H.G., Bae, C.H., Song, S.Y., Kim, Y.D., 2020. Fipronil upregulates inflammatory cytokines and MUC5AC expression in human nasal epithelial cells. Rhinology 58, 66–73.

Li, X.H., Ma, J., Fang, D., Shi, T.R., Gong, Y.W., 2020. Organophosphate flame retardants in soils of Zhejiang Province, China: levels, distribution, sources, and exposure risks. Arch. Environ. Contam. Toxicol. 78, 206–215.

Liu, X., Yu, G., Cao, Z., Wang, B., Huang, J., Deng, S., Wang, Y., 2017. Occurrence of organophosphorus flame retardants on skin wipes: insight into human exposure from dermal absorption. Environ. Int. 98, 113–119.
Liu, X.S., Zhao, X.L., Wang, Y., Hong, J.B., Shi, M., Pfaff, D., Guo, L.X., Tang, H.W., 2020. Triphenyl phosphate permeates the blood brain barrier and induces neurotoxicity in mouse brain. Chemosphere 252, 126470.
Lu, L., Hu, J., Li, G., An, T., 2021. Low concentration Tetrabromobisphenol A (TBBPA) elevating overall metabolism by inducing activation of the Ras signaling pathway. J. Hazard Mater. 416, 125797.
Lu, S.C., 2013. Glutathione synthesis. Biochim. Biophys. Acta 1830, 3143–3153.
Marini, M., Soloperto, M., Mezzetti, M., Fasoli, A., Mattoli, S., 1991. Interleukin-1 binds to specific receptors on human bronchial epithelial cells and upregulates granulocyte/macrophage colony-stimulating factor synthesis and release. Am. J. Respir. Cell Mol. Biol. 4, 519–524.
Marklund, A., Andersson, B., Haglund, P., 2003. Screening of organophosphorus compounds and their distribution in various indoor environments. Chemosphere 53, 1137–1146.
Matsune, S., Ohori, J., Sun, D., Yoshifuku, K., Fukuiwa, T., Kurono, Y., 2008. Vascular endothelial growth factor produced in nasal glands of perennial allergic rhinitis. Am. J. Rhinol. 22, 365–370.
McLaughlin, M., Patin, E.C., Pedersen, M., Wilkins, A., Dillon, M.T., Melcher, A.A., Harrington, K.J., 2020. Inflammatory microenvironment remodelling by tumour cells after radiotherapy. Nat. Rev. Cancer 20, 203–217.
Morry, J., Ngamcherdtrakul, W., Yantasee, W., 2017. Oxidative stress in cancer and fibrosis: opportunity for therapeutic intervention with antioxidant compounds, enzymes, and nanoparticles. Redox Biol. 11, 240–253.
Nian, J.B., Zeng, M., Zheng, J., Zeng, L.Y., Fu, Z., Huang, Q.J., Wei, X., 2020. Epithelial cells expressed IL-33 to promote degranulation of mast cells through inhibition on ST2/PI3K/mTOR-mediated autophagy in allergic rhinitis. Cell Cycle 19, 1132–1142.
Ning, M., Hu, J., Lu, L., Cai, Y., Li, G., An, T., 2020. Toxicity mechanism of tetrabromobisphenol A to human respiratory system cells 16HBE and Beas2B. Chin. Sci. Bull.-Chin. 65, 931–939.
Niture, S.K., Khatri, R., Jaiswal, A.K., 2014. Regulation of Nrf2-an update. Free Radic. Biol. Med. 66, 36–44.
Oyadomari, S., Mori, M., 2004. Roles of CHOP/GADD153 in endoplasmic reticulum stress. Cell Death Differ. 11, 381–389.
Percy, Z., La Guardia, M.J., Xu, Y., Hale, R.C., Dietrich, K.N., Lanphear, B.P., Yolton, K., Vuong, A.M., Cecil, K.M., Braun, J.M., Xie, C., Chen, A., 2020. Concentrations and loadings of organophosphate and replacement brominated flame retardants in house dust from the home study during the PBDE phase-out. Chemosphere 239, 124701.
Phillips, M.J., Voeltz, G.K., 2016. Structure and function of ER membrane contact sites with other organelles. Nat. Rev. Mol. Cell Biol. 17, 69–82.
Qiu, Z., Li, G., An, T., 2021. In vitro toxic synergistic effects of exogenous pollutants-trimethylamine and its metabolites on human respiratory tract cells. Sci. Total Environ. 783, 146915.
Rajendran, P., Nandakumar, N., Rengarajan, T., Palaniswami, R., Gnanadhas, E.N., Lakshminarasaiah, U., Gopas, J., Nishigaki, I., 2014. Antioxidants and human diseases. Clin. Chim. Acta 436, 332–347.
Reisz, J.A., Bansal, N., Qian, J., Zhao, W.L., Furdui, C.M., 2014. Effects of ionizing radiation on biological molecules-mechanisms of damage and emerging methods of detection. Antioxidants Redox Signal. 21, 260–292.
Rizzuto, R., De Stefani, D., Raffaello, A., Mammucari, C., 2012. Mitochondria as sensors and regulators of calcium signalling. Nat. Rev. Mol. Cell Biol. 13, 566–578.
Strandberg, B., Gustafson, P., Soderstrom, H., Barregard, L., Bergqvist, P.A., Sallsten, G., 2006. The use of semipermeable determine persistent membrane devices as passive samplers to organic compounds in indoor air. J. Environ. Monit. 8, 257–262.
Taguchi, K., Yamamoto, M., 2017. The KeAP1-NRF2 system in cancer. Front. Oncol. 7, 85.
Tang, J., Lin, M., Ma, S., Yang, Y., Li, G., Yu, Y., Fan, R., An, T., 2021. Identifying dermal uptake as a significant pathway for human exposure to typical semivolatile organic compounds in an e-waste dismantling site: the relationship of contaminant levels in handwipes and urine metabolites. Environ. Sci. Technol. 55, 14026–14036.
Twig, G., Shirihai, O.S., 2011. The interplay between mitochondrial dynamics and mitophagy. Antioxidants Redox Signal. 14, 1939–1951.
Vandooren, J., Van den Steen, P.E., Opdenakker, G., 2013. Biochemistry and molecular biology of gelatinase B or matrix metalloproteinase-9 (MMP-9): the next decade. Crit. Rev. Biochem. Mol. Biol. 48, 222–272.
Wang, D.M., Wang, Z., Zhang, L., Li, Z.Y., Tian, X.F., Fang, J., Lu, Q.Y., Zhang, X., 2018. Cellular ATP levels are affected by moderate and strong static magnetic fields. Bioelectromagnetics 39, 352–360.
Wang, M., Kaufman, R.J., 2016. Protein misfolding in the endoplasmic reticulum as a conduit to human disease. Nature 529, 326–335.
Wang, Y., Wu, X.W., Zhang, Q.N., Hou, M.M., Zhao, H.X., Xie, Q., Du, J., Chen, J.W., 2017. Organophosphate esters in sediment cores from coastal laizhou bay of the bohai sea, China. Sci. Total Environ. 607, 103–108.
Woehlbier, U., Hetz, C., 2011. Modulating stress responses by the UPRosome: a matter of life and death. Trends Biochem. Sci. 36, 329–337.
Xiang, P., Liu, R.Y., Li, C., Gao, P., Cui, X.Y., Ma, L.Q., 2017. Effects of organophosphorus flame retardant TDCPP on normal human corneal epithelial cells: implications for human health. Environ. Pollut. 230, 22–30.
Yabluchanskiy, A., Ma, Y.G., Iyer, R.P., Hall, M.E., Lindsey, M.L., 2013. Matrix metalloproteinase-9: many shades of function in cardiovascular disease. Physiology 28, 391–403.
Yang, H.P., Magilnick, N., Lee, C., Kalmaz, D., Ou, X.P., Chan, J.Y., Lu, S.C., 2005. Nrf 1 and Nrf2 regulate rat glutamate-cysteine ligase catalytic subunit transcription indirectly via NF-kappa B and AP-1. Mol. Cell Biol. 25, 5933–5946.
Yu, L., Li, N., Zhang, J.S., Jiang, Y., 2017. IL-13 regulates human nasal epithelial cell differentiation via H3K4me3 modification. J. Inflamm. Res. 10, 181–188.
Yu, X., Yin, H., Peng, H., Lu, G., Liu, Z., Dang, Z., 2019. OPFRs and BFRs induced A549 cell apoptosis by caspase-dependent mitochondrial pathway. Chemosphere 221, 693–702.
Yue, C., Ma, S., Liu, R., Yang, Y., Li, G., Yu, Y., An, T., 2022. Pollution profiles and human health risk assessment of atmospheric organophosphorus esters in an e-waste dismantling park and its surrounding area. Sci. Total Environ. 806, 151206.
Zhang, Q., Li, X., Wang, Y., Zhang, C., Cheng, Z., Zhao, L., Li, X., Sun, Z., Zhang, J., Yao, Y., Wang, L., Li, W., Sun, H., 2021. Occurrence of novel organophosphate esters derived from organophosphite antioxidants in an e-waste dismantling area: associations between hand wipes and dust. Environ. Int. 157, 106860.
Zhao, C., Wang, Y., Su, Z., Pu, W., Niu, M., Song, S., Wei, L., Ding, Y., Xu, L., Tian, M., Wang, H., 2020. Respiratory exposure to PM2.5 soluble extract disrupts mucosal barrier function and promotes the development of experimental asthma. Sci. Total Environ. 730, 139145.
Zhao, H.B., Yan, L., Xu, X.G., Jiang, C.M., Shi, J.L., Zhang, Y.W., Liu, L., Lei, S.Z., Shao, D. Y., Huang, Q.S., 2018. Potential of Bacillus subtilis lipopeptides in anti-cancer I: induction of apoptosis and paraptosis and inhibition of autophagy in K562 cells. Amb. Express 8, 16.
Zorova, L.D., Popkov, V.A., Plotnikov, E.Y., Silachev, D.N., Pevzner, I.B., Jankauskas, S. S., Babenko, V.A., Zorov, S.D., Balakireva, A.V., Juhaszova, M., Sollott, S.J., Zorov, D.B., 2018. Mitochondrial membrane potential. Anal. Biochem. 552, 50–59.